

The accretion of brown dwarfs and planets by giant stars – I. Asymptotic giant branch stars

Lionel Siess^{1,2} and Mario Livio^{1*}

¹*Space Telescope Science Institute, 3700 San Martin drive, Baltimore, MD 21218, USA*

²*Laboratoire d'Astrophysique de l'Observatoire de Grenoble, Université Joseph Fourier, B.P. 53X, F-38041, Grenoble Cedex, France*

Accepted 1998 December 9. Received 1998 December 9; in original form 1998 May 18

ABSTRACT

We study the response of the structure of an asymptotic giant branch (AGB) star to the accretion of a brown dwarf or planet in its interior. In particular, we examine the case in which the brown dwarf spirals-in, and the accreted matter is deposited at the base of the convective envelope and in the thin radiative shell surrounding the hydrogen burning shell. In our spherically symmetric simulations, we explore the effects of different accretion rates and we follow two scenarios in which the amounts of injected mass are equal to ~ 0.01 and $\sim 0.1 M_{\odot}$. The calculations show that for high accretion rates ($\dot{M}_{\text{acc}} = 10^{-4} M_{\odot} \text{ yr}^{-1}$), the considerable release of accretion energy produces a substantial expansion of the star and gives rise to hot bottom burning at the base of the convective envelope. For somewhat lower accretion rates ($\dot{M}_{\text{acc}} = 10^{-5} M_{\odot} \text{ yr}^{-1}$), the accretion luminosity represents only a small fraction of the stellar luminosity, and as a result of the increase in mass (and concomitantly of the gravitational force), the star contracts. Our simulations also indicate that the triggering of thermal pulses is delayed (accelerated) if mass is injected at a slower (faster) rate. We analyse the effects of this accretion process on the surface chemical abundances and show that chemical modifications are mainly the result of deposition of fresh material rather than of active nucleosynthesis. Finally, we suggest that the accretion of brown dwarfs and planets can induce the ejection of shells around giant stars, increase their surface lithium abundance and lead to significant spin-up. The combination of these features is frequently observed among G and K giant stars.

Key words: accretion, accretion discs – stars: abundances – stars: AGB and post-AGB – stars: evolution – stars: low-mass, brown dwarfs.

1 INTRODUCTION

The discovery of several extra solar planets and brown dwarf candidates around solar-type stars (e.g. Mayor & Queloz 1995; Butler & Marcy 1996; Cochran et al. 1997; Rebolo et al. 1995, 1996; Basri, Marcy & Graham 1996) has advanced our understanding of the formation of planetary systems, but at the same time has also raised new astrophysical problems. Notably, some of these planets are found to orbit very close to the central star (e.g. Mayor et al. 1997) and their orbits may be tidally unstable. For example, Rasio et al. (1996) showed that the orbital decay of the companion of 51 Peg is inevitable (although on a long time-scale), and the authors conclude that the planet will ultimately spiral-in into the star. Furthermore, the engulfing of planets is certainly a possibility when the star evolves to become a giant (e.g. Livio & Soker 1984). The present paper deals specifically with the reaction of a giant star ‘swallowing’ a massive planet or a brown dwarf. This work was also motivated by the fact that the presence of a binary companion (even

of a substellar mass) has often been invoked to explain the axisymmetrical morphology of elliptical and bipolar planetary nebulae (PNe) (e.g. Iben & Livio 1993; Soker 1992, 1996a; Livio 1997). Notably, if the substellar secondary is not too close to the primary, it will interact with the primary only on the upper asymptotic giant branch (AGB) (e.g. Soker 1995, 1996b).

In the course of its evolution, a main-sequence star climbs along the red giant branch and eventually (at a later stage) can also reach the AGB. During the giant evolutionary phases, a planet may accrete from the wind emitted by the giant or be entirely engulfed by the envelope of the giant. Depending on the initial orbital separation, the planet or brown dwarf may be swallowed during the red giant phase, along the AGB, or survive. Once inside the envelope, owing to viscous friction and also to tidal forces, a fraction of the orbital kinetic energy of the planet is converted into thermal energy and, as a consequence, the binary separation decreases. During this process, orbital angular momentum is imparted to the envelope. The spiraling-in of a planet or a brown dwarf inside the envelope of an AGB star has been studied in several papers (e.g. Livio & Soker 1984; Soker, Harpaz & Livio 1984).

* E-mail: mlivio@stsci.edu

Using simplifying assumptions, these authors were able to follow the evolution of the mass of the brown dwarf subject to accretion and mass loss (evaporation). Their model reveals the existence of a critical mass M_{crit} below which the planet is evaporated or collides with the core. For the particular AGB star model used, they found $M_{\text{crit}} \sim 0.02 M_{\odot}$, but these results must be taken with caution because the physical processes involved in these calculations were treated only approximately. On the observational side, the orbital separations between close binary stars seem to indicate that low-mass secondaries tend to have small orbital separations (e.g. tables 2 and 3 in Iben & Livio 1993). A crude extrapolation of these data to low-mass stars (Soker 1996b) suggests that secondaries with masses of $\leq 0.1 M_{\odot}$ will end up at orbital separations of $\leq 1 R_{\odot}$. As we will see in the next section, it is likely that at these depths inside giants stars, the secondary will be tidally disrupted or evaporated. Consequently, very low-mass secondaries will probably be accreted on to the core of the AGB star.

In the present paper we follow the evolution of an AGB star that accretes matter from the destruction of a brown dwarf or a massive planet, using a spherically symmetric stellar evolution code. In the next section, we present the initial model for the AGB star and the general input physics. In Section 3, we describe the numerical approach and in Section 4 we analyse the results of our computations. The effects of accretion on the nucleosynthesis and surface abundances are presented in Section 5, and a general discussion (Section 6) and summary follow (Section 7).

2 INPUT PHYSICS AND VALUES OF PHYSICAL PARAMETERS

To determine the exact location of the accretion process, we require a knowledge of the structure of the AGB star and the colliding brown dwarf. Where the brown dwarf will disrupt and dissipate can be estimated from the properties of the two objects involved in this scenario. In this section we thus present our initial model for the AGB star and look into the properties of the brown dwarf. With these data at hand, we will try to characterize the accretion process as well as different quantities associated with this phenomenon.

2.1 The AGB star

The initial AGB star model (taken from Forestini & Charbonnel

Table 1. Physical properties of the initial AGB model.

	Envelope	HBS	HeBS	core
$M_{\text{top}} (M_{\odot})$	2.900783	0.545262	0.541040	0.463803
M_{bot}	0.546783	0.544266	0.463803	0
$R_{\text{top}} (R_{\odot})$	198	9.26×10^{-2}	1.92×10^{-2}	1.08×10^{-2}
R_{bot}	0.707	2.49×10^{-2}	1.08×10^{-2}	0
$T_{\text{top}} (10^6 \text{ K})$	3.34×10^{-3}	16.2	78.8	192.2
T_{bot}	2.46	54.7	192.2	135.5
$\rho_{\text{top}} (\text{g cm}^{-3})$	5.785×10^{-9}	0.292	158.4	1.12×10^5
ρ_{bot}	5.14×10^{-4}	115.1	1.12×10^5	2.44×10^6

Table 2. Physical properties of accreting bodies.

$M (M_{\odot})$	$R (R_{\odot})$	$\bar{\rho}_{\text{bd}} (\text{g cm}^{-3})$	$\rho_{\text{c}} (\text{g cm}^{-3})$	$P_{\text{c}} (\text{dyne cm}^{-2})$	$T_{\text{c}} (\text{K})$
0.015	0.095	24.6	147.6	2.4×10^{16}	1.9×10^6
0.10	0.067	468.2	2806.2	4.3×10^{18}	1.8×10^7

1997) has an age of $t_0 = 4.74 \cdot 10^8$ yr. Its initial radius, mass, effective temperature and luminosity are equal to $R = 198 R_{\odot}$, $M = 2.9 M_{\odot}$ (initially $M = 3.0 M_{\odot}$), $T_{\text{eff}} = 3340 \text{ K}$ and $L = 4395 L_{\odot}$, respectively. The star has already undergone two thermal pulses and is in the process of relaxing. The internal structure is composed of a very extended convective envelope, which accounts for more than 99 per cent of the radius. Below the massive convective zone ($M_{\text{env}} \approx 2.36 M_{\odot}$), we find a thin radiative shell surrounding the hydrogen burning shell (HBS). In the HBS, H is mainly burned through the CNO cycle. Below the HBS is the intershell where H is exhausted but where the temperature is too low to allow for helium burning. Below the intershell, helium is efficiently burned through 3α reactions in the so-called helium burning shell (HeBS). At the centre of the star, below the HeBS, the degenerate core is composed mainly of ^{16}O and ^{12}C . The core is highly degenerate and nearly isothermal. In Table 1 we summarize the properties of the AGB star. Note that the maximum temperature occurs off-centre owing to neutrino losses.

2.2 The brown dwarf

Brown dwarfs are compact, low-mass objects ($0.007 M_{\odot} \leq M_{\text{bd}} \leq 0.08 M_{\odot}$) that never undergo efficient hydrogen burning. Their evolution consists of a collapse phase, followed by deuterium burning (for the higher masses) and degenerate cooling (e.g. Stevenson 1991; Burrows et al. 1993). Zepolsky and Salpeter (1969) determined a mass–radius relation for this type of object, given approximately by the interpolation formula

$$\frac{R_{\text{bd}}}{R_{\odot}} \approx 0.105 \left(\frac{2X^{1/4}}{1+X^{1/2}} \right)^{4/3}, \quad (1)$$

where

$$X = \frac{M_{\text{bd}}}{0.0032 M_{\odot}}. \quad (2)$$

Approximating the brown dwarf by a polytropic gaseous sphere with index $n = 1.5$ (characteristic of a non-relativistic degenerate gas), one derives for the central density, pressure and temperature the expressions

$$\rho_{\text{c}} \approx 8.44 \left(\frac{M_{\text{bd}}}{M_{\odot}} \right) \left(\frac{R_{\text{bd}}}{R_{\odot}} \right)^{-3} \text{ g cm}^{-3} \quad (3)$$

$$P_{\text{c}} \approx 8.66 \cdot 10^{15} \left(\frac{M_{\text{bd}}}{M_{\odot}} \right)^2 \left(\frac{R_{\text{bd}}}{R_{\odot}} \right)^{-4} \text{ dyne cm}^{-2} \quad (4)$$

$$T_{\text{c}} \approx 1.7 \cdot 10^7 \mu_{\text{bd}} \left(\frac{M_{\text{bd}}}{M_{\odot}} \right) \left(\frac{R_{\text{bd}}}{R_{\odot}} \right)^{-1} \text{ K}, \quad (5)$$

where μ_{bd} is the mean molecular weight, M_{bd} and R_{bd} are the mass and radius of the brown dwarf, respectively. In Table 2, we present several quantities associated with a brown dwarf and a very low-mass star of 0.015 and 0.1 M_{\odot} , respectively.

A straightforward comparison of the values in Tables 1 and 2 indicates that the mean density of the brown dwarf is of the order of the density encountered in the HBS. It also reveals that brown dwarf radii are of the order of the radius of the hydrogen burning shell.

2.3 Time-scales and orders of magnitude

Given the properties of the AGB star and the brown dwarf, we can now attempt to determine the locus of the brown dwarf dissipation and the ensuing accretion process.

First, we estimate the virial temperature of the brown dwarf, as this represents the temperature above which the thermal kinetic energy of the star can overwhelm the gravitational binding energy of the brown dwarf. This is given by

$$T_v \sim \frac{\mathcal{G} M_{\text{bd}} \mu_{\text{bd}} m_{\text{H}}}{k R_{\text{bd}}} \quad (6)$$

$$\approx 2.3 \cdot 10^6 \mu_{\text{bd}} \left(\frac{M_{\text{bd}}}{0.01 M_{\odot}} \right) \left(\frac{R_{\text{bd}}}{0.1 R_{\odot}} \right)^{-1} \text{ K}. \quad (7)$$

Such temperatures, of the order of a few millions degrees, are encountered at the base of the convective envelope (see Table 1). Therefore, initially relatively massive brown dwarfs ($M \gtrsim 0.01 M_{\odot}$) will probably be able to reach the bottom of the convective envelope without being entirely evaporated. Note that we do not expect the trajectory of the spiraling-in brown dwarf to be strongly affected by the convective motions as its Keplerian velocity is always supersonic (see e.g. Livio & Soker 1984).

As the brown dwarf gets closer to the stellar core, tidal effects become important and they can induce strong distortions to the structure of the brown dwarf, and eventually they can even lead to a total disruption of the brown dwarf. The elongation stress at the brown dwarf centre can be approximated by (e.g. Soker et al. 1987)

$$S = \int_0^{R_{\text{bd}}} \rho_{\text{bd}} \frac{d}{dR} \left(\frac{\mathcal{G}M}{R^2} \right) l dl = \xi \frac{\mathcal{G} \bar{\rho}_{\text{bd}} R_{\text{bd}}^2 M}{R^3} \text{ dyne cm}^{-2}, \quad (8)$$

where $\bar{\rho}_{\text{bd}}$ is the mean density of the brown dwarf, M and R are the mass and radius of the star causing the disruption, and ξ is a parameter of order unity. If we compare this expression with the central pressure of the brown dwarf, then the condition of disruption, $S > P_c$, reads

$$R < \left(\frac{\mathcal{G} \bar{\rho}_{\text{bd}} R_{\text{bd}}^2 M}{P_c} \right)^{1/3} \approx 0.27 \left(\frac{R_{\text{bd}}}{0.1 R_{\odot}} \right)^{2/3} \left(\frac{M}{M_{\odot}} \right)^{1/3} \\ \times \left(\frac{\bar{\rho}_{\text{bd}}}{100 \text{ g cm}^{-3}} \right)^{1/3} \left(\frac{P_c}{10^{17} \text{ dyne cm}^{-2}} \right)^{-1/3} R_{\odot}. \quad (9)$$

From condition (9), it is clear that a disruption of the brown dwarf occurs in regions close to the bottom of the convective envelope. Thus, all the indications are that the brown dwarf will be dissipated (and its material accreted) near the bottom of the convective layer.

In order to estimate the mean accretion rate on to the core of AGB star, we evaluate the orbital decay rate τ_{decay} in the accretion region. The spiraling-in of the brown dwarf is due to the action of drag forces that result from viscous friction and tidal effects. This characteristic time-scale, which is evaluated in the vicinity of the dissipation zone, provides a rough estimate of the transit time-scale of the brown dwarf in this region and the rate at which matter can be deposited there. The accretion time-scale is therefore given approximately by (see e.g. Livio & Soker 1984 for a detailed discussion)

$$\tau_{\text{acc}} = \left(\frac{\dot{a}}{a} \right)^{-1} \approx 162 \left(\frac{M_{\text{bd}}}{0.01 M_{\odot}} \right)^{-1} \left(\frac{r}{0.7 R_{\odot}} \right)^{-3/2} \left(\frac{M}{2 M_{\odot}} \right)^{3/2} \\ \times \left(\frac{\rho}{10^{-4} \text{ g cm}^{-3}} \right)^{-1} \text{ yr}, \quad (10)$$

where ρ is the density in the envelope at radial distance r . Consequently, the expected accretion rate \dot{M}_{acc} is of the order of $\dot{M}_{\text{acc}} \sim M_{\text{bd}}/\tau_{\text{acc}} \approx 6 \cdot 10^{-5} M_{\odot} \text{ yr}^{-1}$ for a $0.01 M_{\odot}$ brown dwarf.

2.4 The accretion process

The previous analysis indicates that a brown dwarf orbiting an AGB star can spiral-in to very deep layers inside the star. On the basis of our estimates of the virial temperature and of tidal effects, we found that the brown dwarf is likely to be dissipated at the base of the convective envelope. The net outcome of the spiraling-in process is therefore the accretion of a brown dwarf mass at rates in the range of $10^{-5} - 10^{-4} M_{\odot} \text{ yr}^{-1}$.

3 NUMERICAL CALCULATIONS

3.1 The stellar evolution code

The stellar evolution code used in the present calculations has been previously used for the computation of grids of standard pre-main-sequence (PMS) evolutionary tracks (Forestini 1994; Siess, Forestini & Dougados 1997a), for the detailed evolution and nucleosynthesis of intermediate mass AGB stars (Forestini & Charbonnel 1997), and also for the effects of disc accretion on to PMS stars (Siess, Forestini & Bertout 1997b, 1998). We refer the reader to these papers for a detailed description of the stellar evolution code.

3.2 The models

We computed two sets of models for two different accretion rates, $\dot{M}_{\text{acc}} = 10^{-4}$ and $10^{-5} M_{\odot} \text{ yr}^{-1}$ (models A and B, respectively). The total accreted mass in cases A and B was $0.01245 M_{\odot}$ and $0.01238 M_{\odot}$, respectively. The chemical composition of the accreted matter was assumed to correspond to a solar metallicity ($Z = 0.02$) with relative abundances from Anders & Grevesse (1989).

Previous works dealing with accretion in different evolutionary phases (e.g. Stahler 1988; Siess et al. 1997b) have pointed out the important role of deuterium in this process. Indeed, the very fast burning of ^2H through the $^2\text{H}(p,\gamma)^3\text{He}$ reaction releases a huge amount of energy that is able to modify the structure and evolution of the star significantly. The presence or absence of deuterium in the accreted matter is thus an important issue, which depends essentially on the mass of the brown dwarf. Brown dwarfs (or planets) more massive than ~ 12 Jupiter masses ($\sim 0.01 M_{\odot}$, e.g. Burrows et al. 1995) have a high enough central temperature to burn deuterium in their interiors. Consequently, we do not expect deuterium to be accreted in the AGB star and its initial mass fraction has been set to be $X_{\text{D}} = 10^{-15}$. We also assume that ^7Li is preserved in the brown dwarf and its mass fraction (abundance) is equal to $X_{\text{Li}} = 9.8968 \cdot 10^{-9}$ [$\log \epsilon(\text{Li}) = 3.31$].

3.3 The deposition of accreted matter

As we discussed in Section 2.4, a sufficiently massive brown dwarf is able to reach the bottom of the convective envelope. The deposition of some accreted matter inside the convective envelope, owing to partial evaporation, will probably not in itself influence the structure as this region is devoid of energy sources. The main effects that need to be studied, therefore, are the consequences of mass deposition in the region close to the bottom of the convective zone, where the planet/brown dwarf is expected to disrupt.

To achieve this goal, we have assumed a simplified mass deposition profile in which the mass $\Delta M_k = M_{k+1} - M_k$ of the shell k is increased at every time step Δt by the amount $f \Delta M_k$, where $f = \dot{M}_{\text{acc}} \Delta t / (M_{\text{top}} - M_{\text{bot}})$. The mass is accreted in the region

delineated by $M_{\text{bot}} < M_r \leq M_{\text{top}}$, where M_{bot} corresponds to the mass coordinate at the top of the HBS. However, if hot bottom burning is taking place (see below), M_{bot} is equal to the bottom of the convective envelope (which is inside the HBS). With this prescription, we allow the accreted matter to go below the convective envelope, but, as we shall see later, a small fraction of the accreted mass (< 5 per cent) is actually deposited in this region. The boundary M_{top} is defined (arbitrarily) as the mass coordinate corresponding to a radius equal to $1 R_{\odot}$ ($M_{\text{top}} \approx 0.55 M_{\odot}$). This accounts for the fact that the planet is actually dissipated in the central region of the star. We also assume that the accreted matter is injected at the temperature and density of the local envelope. This can be justified by the fact that the kinetic energy of the brown dwarf is not too different from the specific thermal energy of the AGB envelope at the same point (e.g. Harpaz & Soker 1994).

In the presence of mass accretion, at each evolutionary time-step, the total mass of the star is increased by the amount $\Delta M = \dot{M}_{\text{acc}} \Delta t$. In the shells where the mass is deposited (for $M_{\text{bot}} < M_r \leq M_{\text{top}}$), the time derivative of a variable $A(M_r, t)$ is now calculated as

$$\left. \frac{DA}{Dt} \right|_{M_r} = \left. \frac{\partial A}{\partial t} \right|_r + (u \nabla) A - \left. \frac{d \ln M}{dt} \frac{\partial A}{\partial \ln \left(\frac{M_r}{M} \right)} \right|_t, \quad (11)$$

where u is the velocity of the shell and $\nabla = \partial/\partial r$. The rate of gravitational energy release, $\varepsilon_{\text{grav}}$, is given by

$$\varepsilon_{\text{grav}} = - \frac{De_{\text{int}}}{Dt} + \frac{P}{\rho^2} \frac{D\rho}{Dt}, \quad (12)$$

where e_{int} is the specific internal energy.

The chemical composition entering the computation at the new time-step is modified owing to the arrival of fresh, not nuclearly processed, material from the accreted matter. The mass fraction $\tilde{X}(t + \Delta t)_{i,k}$ of element i at shell k after mixing, is given by (Siess et al. 1997b)

$$\tilde{X}(t + \Delta t)_{i,k} = \frac{X(t)_{i,k} + f X_i^a}{1 + f}, \quad (13)$$

where $X(t)_{i,k}$ is the stellar mass fraction of element i before mixing and X_i^a is the mass fraction of this element in the accreted matter. Note that X_i^a is constant and does not depend on the mass coordinate.

Finally, in order to speed up the convergence process, we turned off the wind mass loss during the accretion phase and used grey atmosphere models.

4 EVOLUTION OF THE STRUCTURE

The evolution of the AGB star under consideration can be divided into two major phases. The first one deals with the onset of accretion and the main accretion phase, while the second marks the end of the accretion process and the relaxation of the star.

4.1 The onset of accretion and the main accretion phase

The deposition of material inside the star releases a significant amount of gravitational energy. The associated accretion luminosity is given by

$$L_{\text{acc}} = \frac{GM\dot{M}_{\text{acc}}}{R} \approx 5650 \left(\frac{M}{0.54 M_{\odot}} \right) \left(\frac{R}{0.3 R_{\odot}} \right)^{-1} \times \left(\frac{\dot{M}_{\text{acc}}}{10^{-4} M_{\odot} \text{ yr}^{-1}} \right) L_{\odot}. \quad (14)$$

Note that an additional source of energy can arise from the possible replenishment of the nuclearly active region with accreted material. The modification of the chemical composition of these regions can increase the nuclear energy production.

For high accretion rates (case A), L_{acc} represents a large fraction of the stellar luminosity and in the deep region where the energy is deposited, the star expands. Locally, the density, pressure and temperature decrease. The HBS, which advances in mass, rapidly reaches the ‘cooler’ accretion region¹ and then, the nuclear energy production due to H burning decreases (see Fig. 1). On the other hand, the luminosity of the HeBS increases, because the addition of mass results in increased gravity and compressional heating. In the expanding accretion region, the opacity κ increases because in this regime it is a decreasing function of the temperature. The increase in both κ and L (due to L_{acc}) contributes to a steepening of the radiative gradient ($\nabla_{\text{rad}} \propto \kappa L$) that now becomes greater than the adiabatic gradient, thus convection sets in. Consequently, the convective envelope penetrates rapidly towards deeper regions (see Fig. 2) and reaches the HBS, leading to the so-called hot bottom burning (HBB). With the onset of HBB, the luminosity of the HBS (L_{H}) rises sharply, as fresh material coming from the convective region is engulfed in this shell. The global contribution to the total nuclear energy production of the $^{13}\text{C}(p,\gamma)^{14}\text{N}$ reaction is increased during this phase, and it accounts for 27 per cent (compared to 22 per cent in a standard evolution). We also note that the $^{14}\text{N}(p,\gamma)^{15}\text{O}$ and $^{15}\text{N}(p,\alpha)^{16}\text{O}$ reactions contribute less to the nuclear energy production than in a standard scheme. These different features indicate that the CNO cycle is reaching a new equilibrium. The ‘flash’ induced by the penetration of the convective envelope into the HBS increases L_{H} by 4 orders of magnitude. The large release of nuclear energy is used to expand the envelope and shortly after the ignition of the HBB, L_{H} decreases rapidly (Fig. 1). Thereafter, L_{acc} provides most of the luminosity, the HBS almost extinguishes as it moves into the colder accretion region, whereas L_{He} rises as the mass increases. Fig. 3 depicts the profiles of several physical quantities during the early accretion phase. The peaks in the luminosity profiles indicate that the star is not in thermal equilibrium, but rather energy accumulates in its interior. One also notices that this feature is smoothed out as time advances, as a result of the expansion of the star. In our initial model (solid line), the gravitational energy production $\varepsilon_{\text{grav}}$ represents a small fraction of the stellar energy production, 80 per cent of the luminosity is due to nuclear energy. When the accretion process starts (dotted line), $\varepsilon_{\text{grav}}$ increases rapidly below the accretion region as a result of mass deposition. In the accretion region where $\varepsilon_{\text{grav}} < 0$, the expansion induces modifications to the temperature profile, which is now steeper. The nuclear energy production is consequently more localized and concentrated in thinner regions. When HBB starts (short-dashed line), both $\varepsilon_{\text{grav}}$ and ε_{nuc} reach extremum values. The luminosity becomes negative, as most of the energy production is used to expand the star. Finally, when the HBB is settled (long-dashed line), the star heats up in the region of nuclear energy production ($\varepsilon_{\text{grav}} > 0$), whereas expansion proceeds above this zone. During the accretion phase the HBS narrows as the temperature profile becomes steeper (Fig. 2). This also accounts for the global decrease of L_{nuc} over this period. Finally, as mass is being added, all the structural features (location of the maximum energy

¹ For the following discussion, we identify the accretion region as the region located above the HBS and up to a mass coordinate $M_r \approx 0.55 M_{\odot}$ where the mass is deposited. Note also that the top of the accretion region is located in the convective envelope.

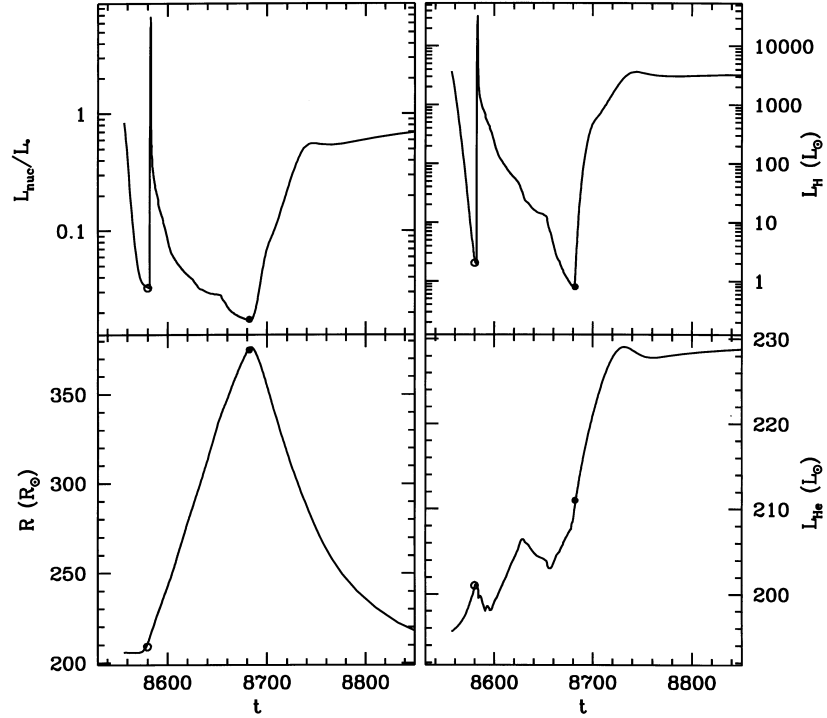


Figure 1. The evolution of the radius (R), nuclear luminosity (L_{nuc}) and nuclear luminosities associated with H (L_{H}) and He (L_{He}) burning, in the case of high accretion rate (case A). Open and filled dots mark the beginning of the hot bottom burning and the end of the accretion process, respectively. In case A, $0.01245 M_{\odot}$ has been accreted in the star.

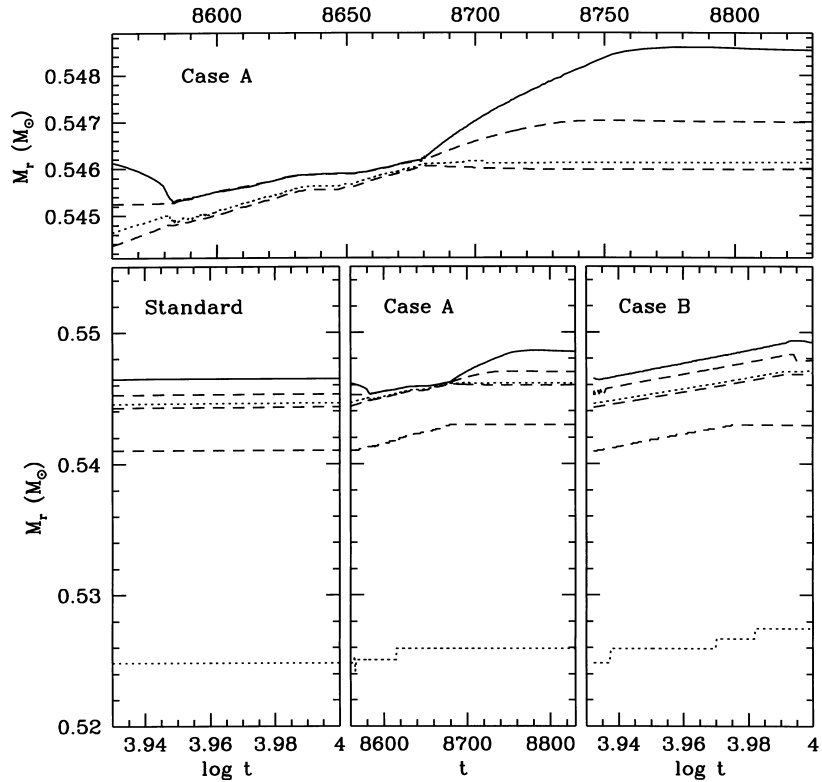


Figure 2. The evolution of the boundaries of the HeBS, HBS and convective envelope. The dotted lines indicate the locus of maximum energy generation while the dashed lines delineate the burning shells ($\epsilon_{\text{nuc}} > 5 \text{ erg g}^{-1} \text{ s}^{-1}$). Note that the bottom of the HeBS has not been marked in the graphs, its location is at about $M_r \approx 0.47 M_{\odot}$. The solid line indicates the lower edge of the convective envelope. The evolution is presented for the standard case (left panel) and for cases A and B (middle and right panels, respectively). The important feature is the appearance of hot bottom burning in case A. The top panel represents an enlarged view of the HBS in case A.

production, burning shells, step in temperature) move towards higher mass coordinates.

In case B, the release of accretion energy is not sufficient to expand the star and trigger convective energy transport down to the HBS. Consequently, a thin radiative layer is maintained below the convective envelope, like in the standard case (Fig. 2). This thin layer prevents the energy production of the HBS from heating the envelope directly and, as L_{acc} is small and the gravitational pull increases, the star contracts. At the beginning of the accretion process, the release of gravitational energy lowers the temperature in the accretion region (above the HBS). As the core grows owing to mass addition, the HBS moves outwards and rapidly penetrates the less dense and cooler accretion region. As a result, the nuclear luminosity due to hydrogen burning (L_{H}) undergoes a sudden drop (Fig. 4). The star compensates for this decrease in energy production by a small contraction. Thereafter, the star tries to find an equilibrium configuration in which L_{nuc} and L_{acc} account for the total luminosity. This phase of structural readjustment leads to a small expansion. Thermal equilibrium is finally achieved after ~ 130 yr, which corresponds to the stellar Kelvin–Helmholtz time-scale

$$\tau_{\text{KH}} \approx 150 \left(\frac{R}{200 R_{\odot}} \right)^{-1} \left(\frac{L}{4500 L_{\odot}} \right)^{-1} \left(\frac{M}{3 M_{\odot}} \right)^2 \text{ yr}. \quad (15)$$

Subsequently, contraction resumes and the nuclear luminosity stays at an almost constant value, somewhat lower than in the standard case (without accretion), owing to the presence of L_{acc} . However, the increase in mass speeds up the contraction rate in the central region and the luminosity of the HeBS rises.

The main difference between case B and the standard evolution is the persistence of stellar contraction, not only in the core but

throughout the entire structure during most of the accretion phase. For low accretion rates, it is mainly the mechanical effects of mass deposition and gravitational attraction that prevail. For a comparison with the high accretion rate case, we present in Fig. 5 the profiles of several physical variables during this period. As can be seen, ϵ_{grav} remains largely positive in the accretion region: contraction heats the central parts of the star. The profiles of T , ϵ_{nuc} and L are very similar during the entire phase. We do not obtain a significant increase in the steepness of the temperature gradient or a peak in the luminosity profile. The different quantities are simply shifted to higher mass coordinates very smoothly. In this case, accretion does not lead to significant structural changes, the energetic effects of accretion (L_{acc}) being too weak.

4.2 The relaxation of the star and the subsequent evolution

For high accretion rates (Fig. 1), the sudden suppression of accretion energy deposition initiates a rapid contraction of the star, as the envelope can no longer be supported. The release of gravitational energy increases the temperature in the regions of energy production and induces an enhancement of the nuclear luminosities. The star globally heats up, the opacity drops, and the convective envelope recedes towards the surface (Fig. 2). The cessation of the accretion process thus marks the end of HBB and this leads to the formation of a thin radiative layer between the convective zone and the HBS. The contraction proceeds as long as the energy losses from the surface are not equilibrated by the gain from gravitational and nuclear energy sources. The return to equilibrium is finally achieved after ~ 675 yr, when the stellar radius and luminosity have decreased by a factor of ~ 2 (Fig. 6). At this point, the nuclear

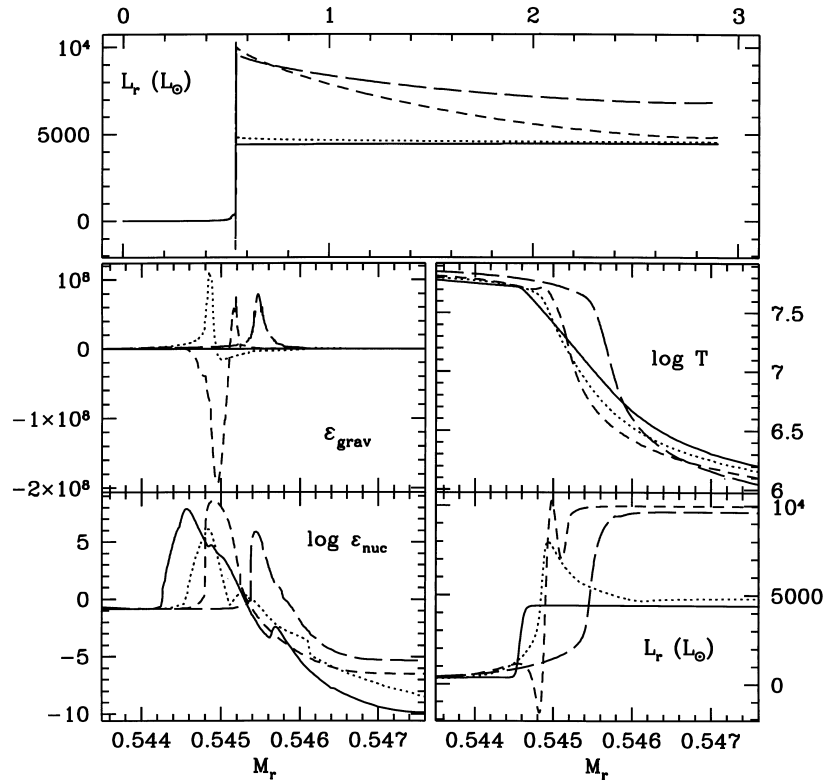


Figure 3. The evolution in the case of high accretion rates of the profiles of gravitational (nuclear) energy production rates ϵ_{grav} (ϵ_{nuc}), temperature (T) and luminosity L_r in the accretion region. The top panel shows the profile of L_r over the entire star. The solid curve refers to our initial model, without accretion. The dotted, short- and long-dashed lines correspond to models for which accretion is taking place for 15, 27 and 67 yr, respectively.

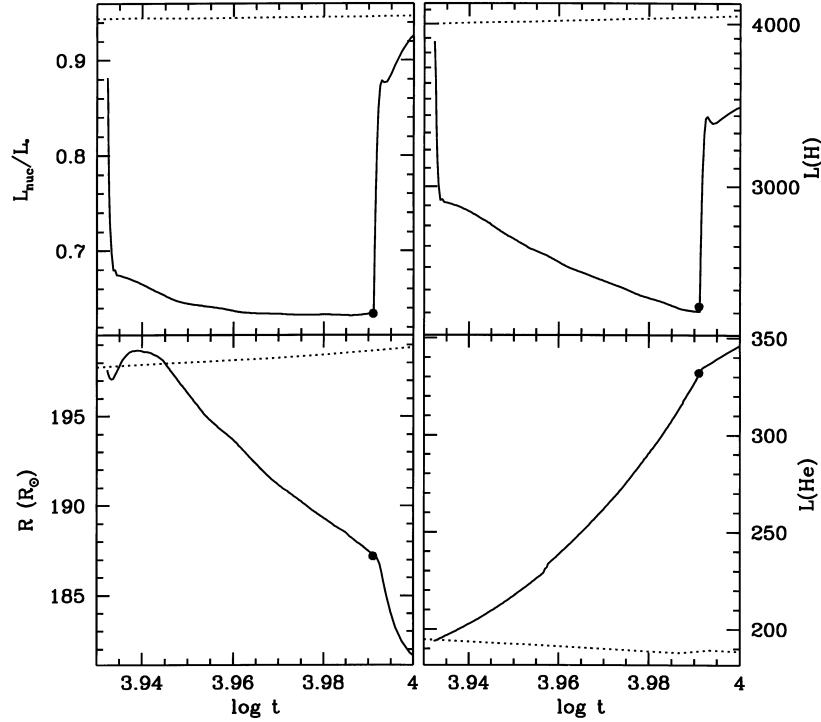


Figure 4. The evolution of the radius (R), nuclear luminosity (L_{nuc}) and nuclear energy production due to H (L_{H}) and He (L_{He}) burning. The solid line refers to case B, the dotted line to the standard model. Filled circles mark the end of the accretion phase.

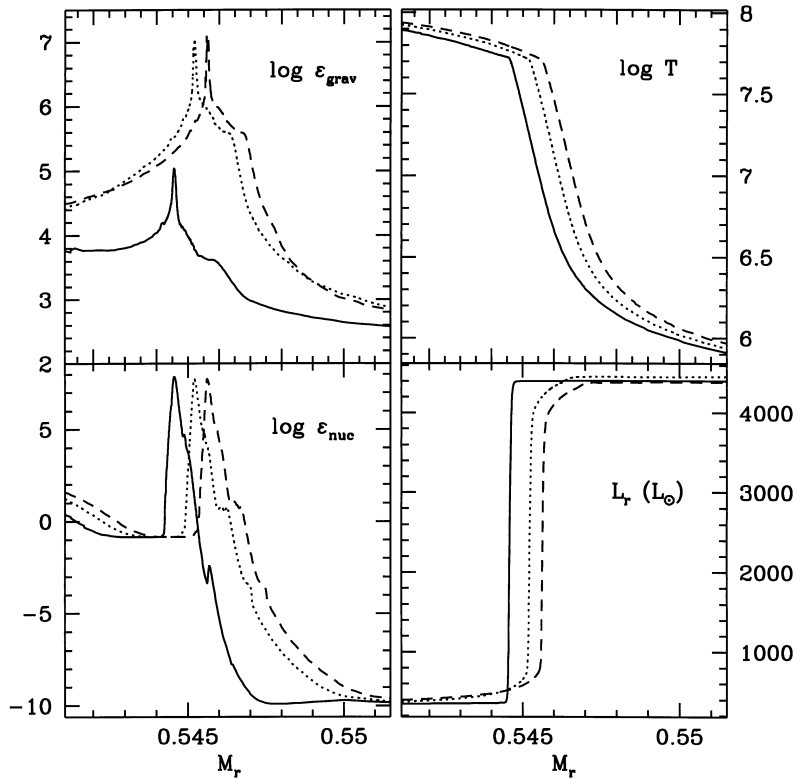


Figure 5. The evolution (in the case of low accretion rates) of the profiles of luminosity (L_r), gravitational (nuclear) energy production rates ϵ_{grav} (ϵ_{nuc}) and temperature (T) in the accretion region. The solid curves refer to our initial model, without accretion. The dotted and short-dashed lines correspond to models for which accretion is taking place for 327 and 535 yr, respectively.

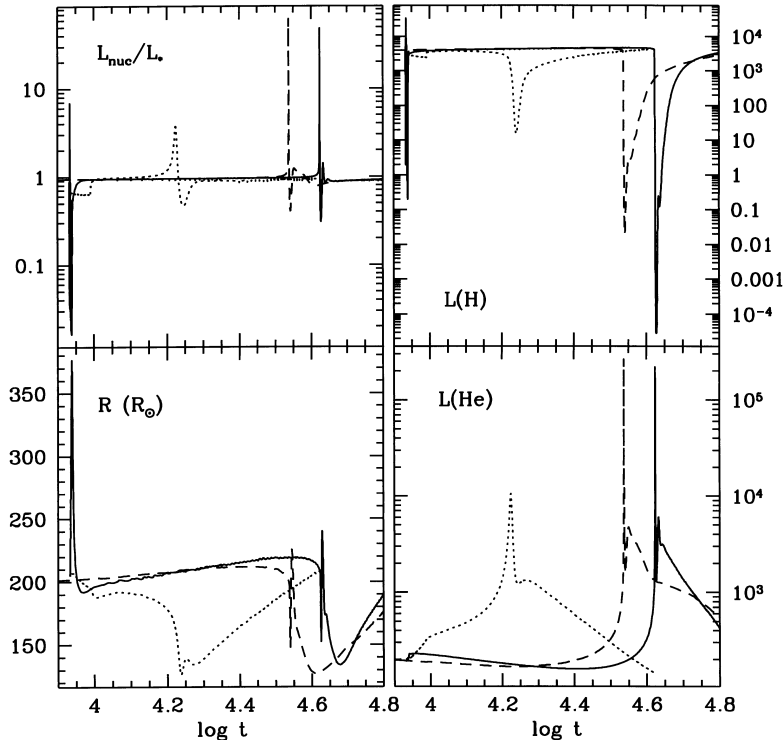


Figure 6. Relaxation of the star. The variables are the same as in Fig. 4. The solid, dotted and dashed lines refer to cases A, B and the standard evolution models, respectively.

luminosity provides more than 90 per cent of the stellar luminosity and it is sufficient to support the envelope. As most of the nuclear energy is produced by the HBS, the energetic influence of the HeBS is shielded and its luminosity (L_{He}) decreases (as in the standard case). Finally, as the core mass M_{core} grows, the temperature inside the HeBS increases and the nuclear reactions (which are very temperature sensitive) runaway and trigger a thermal instability. Note that in case A, the thermal pulse is delayed with respect to the standard model. This is due to the large expansion that occurs during the accretion phase, which in turn slows down the ‘natural’ temperature increase of the HeBS substantially.

In case B, when the accretion process stops, the star undergoes a short phase of rapid contraction with the disappearance of L_{acc} . The temperature in the HBS increases and the nuclear luminosity rises (Fig. 6). For a short period of time the star expands. Finally, when an equilibrium configuration is reached, which accounts for the missing L_{acc} , the star resumes contraction and L_{He} keeps rising. The tendency of increasing L_{He} is due to the fact that for low accretion rates the impact of accretion is more a consequence of the mechanical effects resulting from mass deposition (compressional heating), than energetic effects owing to L_{acc} or HBB. Note in addition that the accretion rate used in this study is larger than the ‘normal’ core growth rate ($\sim 10^{-7} M_{\odot} \text{yr}^{-1}$, for a $3 M_{\odot}$ star). Therefore, accretion forces the star to evolve more rapidly than in a standard evolution and the thermal pulse occurs earlier. However, the thermal instability is weaker in the star accreting the brown dwarf than in the standard model: the maximum of L_{He} is more than an order of magnitude lower than in the conventional computation. The reason for this difference is the fact that owing to the mass deposition, the HeBS moves towards regions of a lower density faster than in the standard scheme, and the nuclear energy generation is thus reduced.

4.3 Accretion of more massive bodies

If a high accretion rate ($\dot{M}_{\text{acc}} = 10^{-4} M_{\odot} \text{yr}^{-1}$) is sustained for a longer period of time, the release of gravitational energy maintains the envelope expansion. After ~ 240 yr, the Kelvin–Helmholtz time-scale has decreased to ~ 60 yr and accretion energy can now be efficiently radiated away. At that time, the nuclear energy production is at a minimum and the HBS is almost extinguished (Fig. 7). The luminosity profile is now monotonically increasing and contraction resumes. When the accretion process ends (for an accreted mass $M_{\text{acc}} = 0.0594 M_{\odot}$ in this simulation), the contraction rate accelerates as the envelope is no longer supported by the deposition of accretion energy. The temperature increases and L_{He} rises first, followed by L_{H} . When the nuclear sources provide ≥ 90 per cent of the stellar luminosity, the contraction stops. The radius is then minimal and its value is smaller than in case A, because in this simulation, the stellar mass and thus the gravitational pull are larger. Finally, as the temperature increases, the thermal instability sets in, but somewhat later than in case A.

For lower accretion rates ($\dot{M}_{\text{acc}} = 10^{-5} M_{\odot} \text{yr}^{-1}$), the persistent addition of mass, up to $M_{\text{acc}} = 0.1082 M_{\odot}$, increases the contraction rate. The star heats up faster and the thermal instability develops even earlier than in case B (Fig. 8). For the reasons explained previously (see Section 4.2), the value of L_{He} during the pulse is lower than in the standard case. We also note that accretion does not perturb the thermal pulse, which indicates that in this case this process represents a small perturbation to the stellar structure. When the instability is over, the star resumes contraction. The nuclear luminosity (L_{nuc}) is lower than in the standard model because a fraction of the energy is provided by the accretion process. Finally, when accretion ends, the star relaxes and returns to a standard evolution (with a larger mass however).

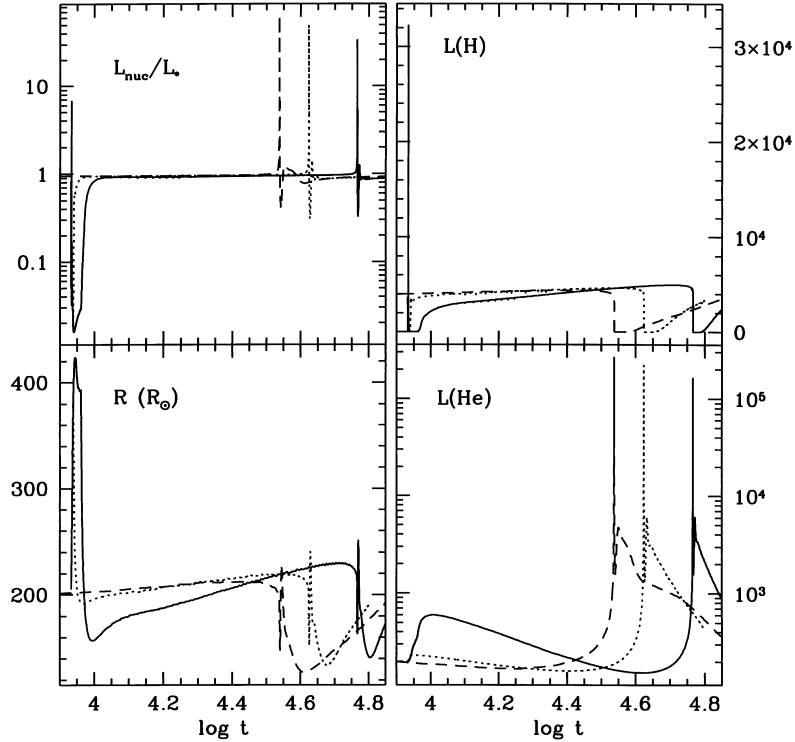


Figure 7. The influence of mass deposition for high accretion rates ($10^{-4} M_{\odot} \text{ yr}^{-1}$). The physical quantities are the same as in Fig. 4. The solid curves correspond to a long-lasting accretion phase ($M_{\text{acc}} = 0.0594 M_{\odot}$), the dotted line to case A ($M_{\text{acc}} = 0.01245 M_{\odot}$) and the dashed line is the standard model.

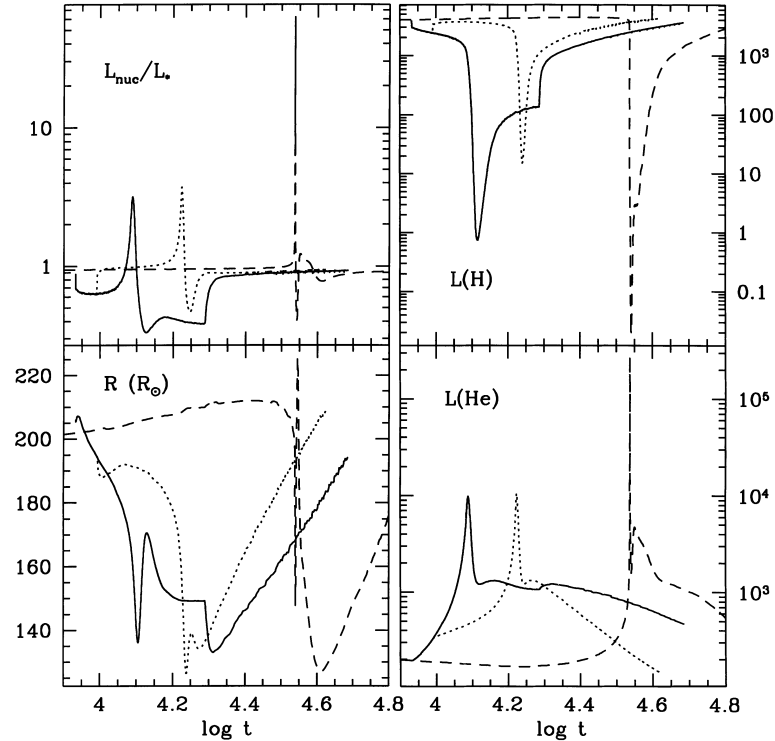


Figure 8. Same as Fig. 7 but for low accretion rates ($10^{-5} M_{\odot} \text{ yr}^{-1}$). The solid curves correspond to $M_{\text{acc}} = 0.1082 M_{\odot}$, the dotted lines to case B ($M_{\text{acc}} = 0.01238 M_{\odot}$) and the dashed lines represent the standard model.

To summarize these simulations, for high accretion rates the accretion luminosity dominates the stellar energetics, reducing the nuclear energy production of the HBS. As a result, the (nuclear) evolution of the star is slowed down. For lower accretion rates (but

still high compared with the normal core growth rate), accretion shifts the internal structure to that corresponding to higher masses at a faster rate than in a standard evolution, and consequently the evolution is accelerated. However, these results do not imply that

for some intermediate value of \dot{M}_{acc} the evolution of the star remains unchanged. Indeed, the stellar mass increases and the growth rate of the core remains always higher than in a standard evolution. In the limiting case, where the release of accretion energy exactly counterbalances the gravitational attraction, instantaneously the evolution of the star would remain the same. However, this situation is unstable since M_{core} increases. Quite rapidly the gravitational pull takes over and the contraction resumes. Note that for large accretion rates when the accretion process is maintained for a longer period of time, contraction finally resumes once thermal equilibrium is reached.

5 SURFACE ABUNDANCES AND NUCLEOSYNTHESIS

Chemical modifications resulting from mass accretion are expected if either a substantial amount of accreted matter is deposited in the envelope or/and nuclear burning is operating in the convective envelope. To separate these two effects, we define new variables R_1 and R_2 for each chemical element i by

$$R_{1,i} = \frac{\tilde{X}_i(t)}{X_i^s(t)} \quad (16)$$

$$R_{2,i} = \frac{\tilde{X}_i(t)}{(X_i^s(t) + m_{\text{acc}} X_i^a)/(1 + m_{\text{acc}})}, \quad (17)$$

where $\tilde{X}_i(t)$ is the mass fraction of element i in an evolutionary scheme with accretion and $X_i^s(t)$ is the mass fraction of this element in standard computations. m_{acc} represents the ratio of the total mass deposited in the envelope during the accretion process ($M_{\text{acc,env}}$) to

the mass of this region (M_{env}). The variable R_1 describes the effect of accretion on the surface abundances, including mass deposition and nuclear burning. The variable R_2 represents the nuclear activity: it gives the ratio of the mass fraction computed in our models with accretion to the mass fraction expected from calculations with accretion if no nuclear burning took place. Therefore, if the element is nucleary produced, then $R_2 > 1$ and if it is destroyed, $R_2 < 1$.

The deposition of fresh, nuclearly unaltered material in the convective envelope entails modifications of the surface chemical abundances. This effect accounts for the large values of R_1 attached to light elements such as ${}^6\text{Li}$, ${}^7\text{Li}$, ${}^9\text{Be}$, ${}^{10}\text{B}$ or ${}^{11}\text{B}$ (Fig. 9). Indeed, owing to their low burning temperature, these elements were previously burned during the pre-main-sequence phase or during the first dredge-up. Depending on the mass added to the envelope, the abundances of these elements can be increased by a factor of $\sim 2 - 8$ (0.3 - 0.9 dex). The more mass that is accreted, the higher the ratio R_1 is. However, the detection of these chemical changes may be difficult if the accreted mass is small. For example, the ${}^7\text{Li}$ mass abundance in cases A and B ($M_{\text{acc,env}} \sim 0.01 M_{\odot}$) reaches values of $\log \epsilon(\text{Li}) = 1.54$ and $\log \epsilon(\text{Li}) = 1.51$, respectively, which are very close to the $\log \epsilon(\text{Li}) = 1.40$ standard value. It is interesting to note that the accretion of planetary material in the envelope of red giant stars was originally suggested by Alexander (1967) to explain the high Li abundance observed in some red giants. Brown et al. (1989) showed that a sufficient mass of terrestrial-like planets (which have lost their initial H and He content) may replenish the envelope of giants sufficiently to reproduce high observed Li abundances. Note, finally, that the surface abundances of heavier elements, with $A > 13$, are close to their initial values and are thus not modified by the accretion process.

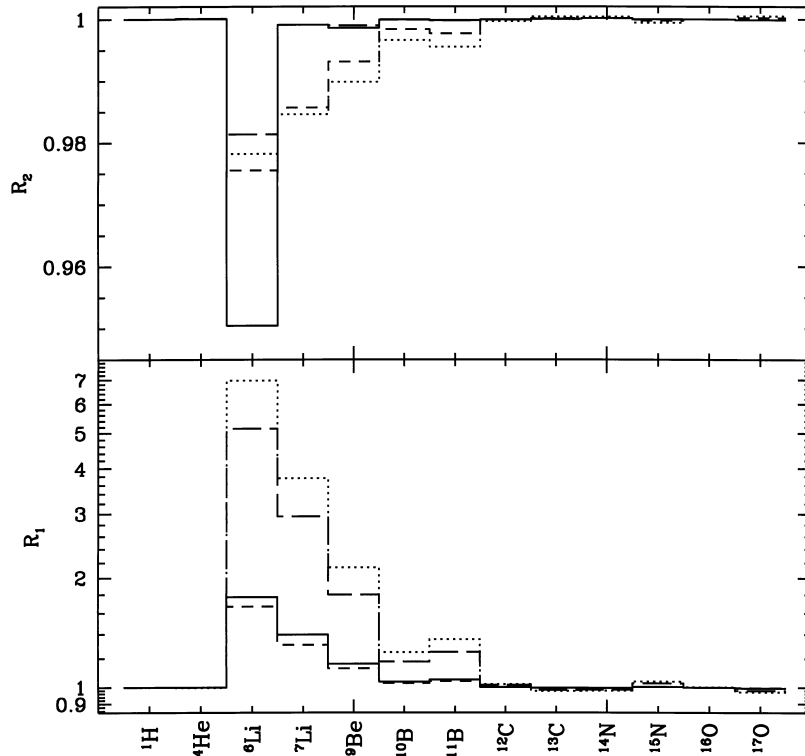


Figure 9. The effects of accretion on the surface abundances of several chemical elements. The lower panel shows the ratio of the mass fraction of an element resulting from our computations with accretion to the standard value. The solid and short-dashed lines correspond to cases A and B, respectively. The dotted and long-dashed lines correspond to longer accretion phase, with accretion rates (accreted masses) that are equal to 10^{-4} ($0.0594 M_{\odot}$) and $10^{-5} M_{\odot} \text{yr}^{-1}$ ($0.1082 M_{\odot}$), respectively. The upper panel represents the nuclear activity. If $R_2 > 1$ ($R_2 < 1$) the element is nucleary produced (destroyed, see text).

The upper panel of Fig. 9 indicates which elements undergo efficient nuclear reactions. The light elements are the principal target of nuclear burning. Indeed the ‘low’ temperature at the base of the convective region, between 3×10^6 and 10^7 K (depending on the presence or absence of HBB), allows the destruction of these species. The nuclear burning acts preferentially on ${}^6\text{Li}$, ${}^7\text{Li}$ and ${}^9\text{Be}$. We can also detect the effects of CNO reactions in the envelope through the production of ${}^{13}\text{C}$, ${}^{14}\text{N}$ and ${}^{17}\text{O}$ and the depletion of ${}^{12}\text{C}$. However, the influence of H burning through the CNO cycle is very small and it only appears if accretion is maintained for a sufficiently long period of time (dotted and dashed lines in Fig. 9).

To summarize, the temperature at the base of the convective envelope ($\leq 10^7$ K) is too low to give rise to a rich nucleosynthesis. The main chemical changes thus result from the deposition of fresh material in the convective envelope.

6 DISCUSSION

Our computations involved a relatively young AGB star (at the beginning of the thermally pulsing phase) and one may wonder what would be the effects of brown dwarf accretion inside more evolved stars. In this respect we note, that as the evolution progresses, the core grows but the temperature at the base of the convective zone remains almost constant, close to 4×10^6 K. Thus, the location of the accretion process may remain unchanged. However, in older AGB stars the stellar luminosity is substantially higher and this will most certainly result in a different stellar response to high accretion rates. Indeed, as we have seen in the present work, the main reason for the stellar expansion is the release of a large amount of accretion energy ($L_{\text{acc}} > L_*$). We thus expect that if mass is injected in more luminous AGB stars, then the stellar radius and luminosity will decrease during the process, as in case B (see also Harpaz & Soker 1994).

Our calculations revealed that for high mass injection rates ($\dot{M}_{\text{acc}} = 10^{-4} M_{\odot} \text{yr}^{-1}$) the radius and luminosity of the star increase by a factor of ~ 2 . This leads to a substantial increase in the mass-loss rate, as according to the Reimers formula (1975) $\dot{M}_{\text{loss}} \propto LR/M$. The ejected mass can be estimated as

$$M_{\text{eject}} \sim 10^{-4} \left(\frac{L}{5000 L_{\odot}} \right) \left(\frac{R}{200 R_{\odot}} \right) \left(\frac{M}{M_{\odot}} \right)^{-1} \left(\frac{t_{\text{acc}}}{100 \text{ yr}} \right) M_{\odot}, \quad (18)$$

where t_{acc} is the duration of the accretion process. We can therefore expect the formation of shells, corresponding to individual accretion events. The mass of these shells is of the order of $\sim 10^{-3} - 10^{-4} M_{\odot}$.

A phenomenon not directly addressed by our spherically symmetric calculations is that of the deposition of angular momentum into the envelope of the giant, by the accreted brown dwarf. We can however estimate the effects of such a deposition as follows. If we assume that the secondary deposits all of its orbital angular momentum in the envelope, and we further assume that the envelope rotates rigidly (owing to the fact that it is convective, and thus viscous) then the ratio of the envelope angular velocity ω to the critical velocity (surface Keplerian angular velocity) ω_{K} is given by

$$\frac{\omega}{\omega_{\text{K}}} \approx 0.085 \left(\frac{M_{\text{bd}}}{0.01 M_{\text{env}}} \right) \left(\frac{a}{R} \right)^{1/2}, \quad (19)$$

where a is the initial orbital radius of the brown dwarf. Here we calculated the moment of inertia of the envelope for our model, and it is given by $I_{\text{env}} = k^2 M_{\text{env}} R^2$, where $k^2 \approx 0.12$. As we can see, equation (19) indicates that for typical brown dwarf masses, the

AGB star can be spun-up to a significant fraction of the critical velocity. Notably, the accretion of angular momentum is required to explain the abnormally high rotational velocities of FK Comae stars (e.g. Rucinski 1990; Welty & Ramsey 1994) and of peculiar AGB stars such as V Hydrae (Barnbaum, Morris & Kahane 1995). Finally, this can also have important consequences for the shaping of planetary nebulae (see e.g. Soker 1996a). In particular, it has been suggested that the spin-up of the envelope is responsible for the high fraction of non-spherical planetary nebulae (see Livio 1997 for a review).

Concerning peculiar abundances, the discovery of lithium-rich G and K giant stars (e.g. Wallerstein & Sneden 1982; Brown et al. 1989; de la Reza & da Silva 1995) posed the problem of the origin of this element in these stars. Indeed, standard stellar evolution predicts that Li should be depleted during the pre-main-sequence phase or during the first dredge-up. Several mechanisms have been proposed to explain the high Li abundance. These include: (1) Li production (Cameron & Fowler 1971), (2) the retainment of the original lithium, (3) the external enrichment by novae (e.g. Gratton & D’Antona 1989), (4) the engulfing of a planet (e.g. Brown et al. 1989). Recently, de la Reza et al. (1996, 1997) pointed out that almost all the Li K giants are optical counterparts of *IRAS* sources, the far-IR excesses being attributed to the presence of a dusty circumstellar shell (CS). Based on this apparent correlation between the IR and Li excesses, these authors proposed a scenario in which all the K giants with masses between 1.0 and $2.5 M_{\odot}$ become Li rich after the first dredge-up. They assume that the mechanism responsible for the Li enrichment is accompanied by a sudden mass loss, which leads to the formation of a CS. The Li that has not been ejected remains in the stellar surface and is depleted later when the mass loss stops. In this scenario, the CS expands, cools down, disappears and the Li surface abundance reaches standard values again. This evolutionary path, or ‘Li path’, can reasonably explain the Li abundance distribution of K giant stars in a colour–colour diagram. Its duration is of the order of $\sim 10^5$ yr and it requires that Li suddenly appears at the surface of the star and then is depleted on a time-scale of $10^3 - 10^5$ yr. However, de la Reza et al. do not provide convincing mechanisms for Li enrichment and mass loss. They invoke an extra mixing process for Li production, the ‘cool bottom processing’ (Wasserburg, Boothroyd & Sackmann 1995), but they remain vague about the generation of mass loss. We propose here that the accretion of a planet or a brown dwarf by a giant star could effectively explain all of these features. Indeed, our calculations show that the accretion process (1) can increase the mass-loss rate and lead to the ejection of a shell (equation 18), and (2) can enrich the envelope with lithium (Fig. 9), in agreement with observations.

Observations also show that lithium rich giants have generally normal rotational velocities [de Medeiros, Melo & Mayor 1996; although some rapid rotators exist, e.g. 1E 1751+7046 (Ambruster et al. 1997)]. This implies that if the accretion of a planet/brown dwarf is responsible for the Li enhancement, some fraction of the orbital angular momentum that is deposited into the envelope has to be removed (or in most cases of engulfed planets $a/R < 1$, see equation 19). This can be achieved by efficient magnetic braking, as the giants develop a deep convective envelope (e.g. Leonard & Livio 1995). We should note that the paucity of giants showing both rapid rotation and high Li abundance probably indicates that the time-scale for rotational braking is short compared with the giant evolutionary phase (a few 10^7 yr).

The existence of very rich Li stars (e.g. Gregorio-Hetem et al. 1992; Torres et al. 1995; de la Reza & da Silva 1995; Fekel et al.

1996) poses a somewhat more difficult challenge. One could imagine, however, that the collision of the planet (or a brown dwarf) with the core of the star may trigger the ‘cool bottom processing’ (Wasserburg et al. 1995). In this scenario, ${}^7\text{Be}$ -rich material can be dredged-up from the deep interior to the convective envelope where it decays through the ${}^7\text{Be}(e^-, \nu){}^7\text{Li}$ reaction.

A comment should be added about statistics. From a sample of 644 stars, Brown et al. (1989) found that ~ 4 per cent of G and K giants have Li abundances above $\log \epsilon(\text{Li}) \sim 1.3$ and that an additional 4 per cent have abundances between 1.2 and 1.3. Considering the fact that many of the Li rich stars show an IR excess compatible with the presence of a surrounding shell, it is tempting to interpret these observations as a signature of an accretion event. This could indicate that 4 – 8 per cent of all stars have low-mass (possibly substellar) companions. These statistics are fully compatible with those inferred from PNe nuclei (e.g. Yungelson, Tutukov & Livio 1993).

7 SUMMARY

We have presented computations in which a brown dwarf (or a planet) is accreted in the core of an AGB star. This situation results when the brown dwarf is engulfed in the stellar envelope as the latter is expanding owing to stellar evolution. Viscous friction as well as tidal effects generate a drag force that makes the brown dwarf spiral-in. We have shown that the region where the brown dwarf is expected to disrupt is close to the base of the convective envelope.

We investigated the response of the star to the accretion of a small body for two accretion rates, 10^{-4} and $10^{-5} M_{\odot} \text{yr}^{-1}$. Our simulations show that for the higher accretion rate, the main energetic effects come from the release of potential energy. The accretion luminosity is of the order of the stellar luminosity and this additional energy source makes the star expand. Another interesting feature of these computations (involving a high accretion rate) is the appearance of hot bottom burning. However, the relatively low temperature at the base of the convective envelope ($\sim 10^7$ K) and the short duration of the accretion phase do not allow for a rich nucleosynthesis in the convective zone. We find that accretion delays the development of the thermal instability. The nuclear energy production resulting from the H and He burning shells is smaller than in a standard case because a part of the energy is provided by the deposition of the accretion energy. Hydrogen and helium are consequently burned more slowly and the evolution is slowed down.

For the lower accretion rate the evolution is different. In this case the accretion luminosity represents a small fraction of the stellar luminosity and therefore expansion does not ensue. Conversely, the addition of mass increases the gravitational pull and the star contracts even more efficiently than in a standard scheme. The temperature of the nuclear burning shells increases more rapidly and the thermal instability occurs earlier than in conventional evolution. The global stellar evolution is accelerated.

Except for variations in the luminosity and radius, both of which can be increased by a factor of ~ 2 , the effects of mass accretion in an evolved star may be traced by changes in the surface chemical abundances. We showed that such changes are mainly the result of material deposition rather than nucleosynthesis. The chemical changes affect mainly light elements such as ${}^7\text{Li}$ and ${}^9\text{Be}$, the mass fraction of which can be increased by a factor of 2–8, depending on the accretion rate and duration of the accretion process.

Generally, the observational signatures of the accretion of a

brown dwarf or a planet by giant stars can be (depending on the physical parameters involved): (i) the formation of a circumstellar shell, (ii) the enhancement of the surface ${}^7\text{Li}$ abundance, (iii) rapid rotation. We propose that the IR excesses and high Li abundances observed in 4 – 8 per cent of the G and K giants originate from the accretion of massive planets/brown dwarfs/very low-mass stars.

Finally, we should note that we also made several attempts to accrete matter deeper inside the star (e.g. below the HBS). However, such a process could not be followed reliably with our code. The deposition of protons in the very central regions increases the nuclear energy production to such rates that the envelope cannot absorb this energy excess.

ACKNOWLEDGMENTS

LS wishes to thank Manuel Forestini for invaluable discussions and also for kindly providing us with the initial stellar model. LS acknowledges support from the French Ministry of Foreign Affairs (Bourse Lavoisier) and thanks the STScI for its hospitality. This work has been supported in part by NASA grants NAGW-2678, G005.52200 and G005.44000, and the Director’s Discretionary Research Fond at STScI. The computations presented in this paper were performed at the ‘Centre Intensif de Calcul de l’Observatoire de Grenoble’.

REFERENCES

- Alexander J. B., 1967, *Observatory*, 87, 238
 Ambruster C. W., Fekel F. C., Guinan E. F., Hrivnak B. J., 1997, *ApJ*, 479, 960
 Anders E., Grevesse N., 1989, *Geochim. Cosmochim. Acta*, 53, 197
 Basri G., Marcy G. W., Graham J. R., 1996, *ApJ*, 458, 600
 Barnbaum C., Morris M., Kahane C., 1995, *ApJ*, 450, 862
 Burrows A., Hubbard W. B., Saumon D., Lumine J. I., 1993, *ApJ*, 406, 158
 Burrows A., Saumon D., Guillot T., Hubbard W. B., Lumine J. I., 1995, *Nat*, 375, 299
 Butler R. P., Marcy G. W., 1996, *ApJ*, 464, L153
 Brown J. A., Sneden C., Lambert D. L., Dutchover E. Jr, 1989, *ApJS*, 71, 293
 Cameron A. G. W., Fowler W. A., 1971, *ApJ*, 164, 11
 Cochran W. D., Hatzes A., Butler R. P., Marcy G. W., 1997, *ApJ*, 483, 457
 de la Reza R., da Silva L., 1995, *ApJ*, 439, 917
 de la Reza R., Drake N. A., da Silva L., 1996, *ApJ*, 456, L115
 de la Reza R., Drake N. A., da Silva L., Torres C. A. O., Martin E. L., 1997, *ApJ*, 482, L77
 de Medeiros J. R., Melo C. H. F., Mayor M., 1996, *A&A*, 309, 465
 Fekel F. C., Webb R. A., White R. J., Zuckerman B., 1996, *ApJ*, L95
 Forestini M., 1994, *A&A*, 285, 473
 Forestini M., Charbonnel C., 1997, *A&AS*, 123, 241
 Gratton R. G., D’Antona F., 1989, *A&A*, 215, 66
 Gregorio-Hetem J., Lepine J. R. D., Quast G. R., Torres C. A. O., de la Reza R., 1992, *AJ*, 103, 549
 Harpaz A., Soker N., 1994, *MNRAS*, 270, 734
 Iben I. Jr, Livio M., 1993, *PASP*, 105, 1373
 Leonard P. T. J., Livio M., 1995, *ApJ*, 447, L21
 Livio M., 1997, *Space Sci. Rev.*, in press
 Livio M., Soker N., 1984, *MNRAS*, 208, 763
 Mayor M., Queloz D., 1995, *Nat*, 378, 355
 Mayor M., Queloz D., Udry S., Halbwachs J.-L., 1997, in *Cosmovici C., Bowyer S., Werthimer D., eds. Proc. 5th Int. Conf. on Bioastronomy, IAU Coll. 161 Editrice Compositori, Bologna*, p. 313
 Rasio F. A., Tout C. A., Lubow S. H., Livio M., 1996, *ApJ*, 470, 1187
 Rebolo R., Zapatero-Osorio M. R., Martin E. L., *Nat*, 1995, 377, 129
 Rebolo R., Martin E. L., Basri G., Marcy G., Zapatero-Osorio M. R., 1996, *ApJ*, 469, L53
 Reimers D., 1975, *Men. Soc. Roy. Sci. Liège*, 6th Ser. 8, 369

- Rucinski S. M., 1990, *PASP*, 102, 306
Siess L., Forestini M., Dougados C., 1997a, *A&A*, 324, 556
Siess L., Forestini M., Bertout C., 1997b, *A&A*, 326, 1001
Siess L., Forestini M., Bertout C., 1998, *A&A*, in press
Soker N., 1992, *ApJ*, 389, 628
Soker N., 1995, *MNRAS*, 274, 147
Soker N., 1996a, *ApJ*, 460, L53
Soker N., 1996b, *ApJ*, 468, 774
Soker N., Harpaz A., Livio M., 1984, *MNRAS*, 210, 189
Soker N., Regev O., Livio M., Shara M. M., 1987, *ApJ*, 318, 760
Stahler S. W., 1988, *ApJ*, 332, 804
Stevenson D. J., 1991, *ARA&A*, 29, 163
Torres C. A. O., Quast G. R., de la Reza R., Gregorio-Hetem J., Lepine J. D., 1995, *AJ*, 109, 2146
Wallerstein G., Sneden C., 1982, *ApJ*, 225, 577
Wasserburg G. J., Boothroyd A. I., Sackmann I. J., 1995, *ApJ*, 447, L37
Welty A. D., Ramsey L. W., 1994, *ApJ*, 435, 848
Yungelson L. R., Tutukov A. V., Livio M., 1993, *ApJ*, 418, 794
Zapolsky H. S., Salpeter E. E., 1969, *ApJ*, 158, 809

This paper has been typeset from a $\text{T}_E\text{X}/\text{L}^A\text{T}_E\text{X}$ file prepared by the author.